nature nanotechnology

LETTERS

PUBLISHED ONLINE: 11 AUGUST 2013 | DOI: 10.1038/NNANO.2013.150

Quantum interference in plasmonic circuits

Reinier W. Heeres*, Leo P. Kouwenhoven and Valery Zwiller

Surface plasmon polaritons (plasmons) are a combination of light and a collective oscillation of the free electron plasma at metal/dielectric interfaces[1]. This interaction allows subwavelength confinement of light beyond the diffraction limit inherent to dielectric structures[2]. As a result, the intensity of the electromagnetic field is enhanced, with the possibility to increase the strength of the optical interactions between waveguides, light sources[3–6] and detectors[7,8]. Plasmons maintain non-classical photon statistics[9,10] and preserve entanglement upon transmission through thin, patterned metallic films[11,12] or weakly confining waveguides[13]. For quantum applications[3,14], it is essential that plasmons behave as indistinguishable quantum particles. Here we report on a quantum interference experiment in a nanoscale plasmonic circuit consisting of an on-chip plasmon beamsplitter with integrated superconducting single-photon detectors[15] to allow efficient single plasmon detection[16]. We demonstrate a quantum-mechanical interaction between pairs of indistinguishable surface plasmons by observing Hong–Ou–Mandel (HOM) interference[17], a hallmark non-classical interference effect that is the basis of linear optics-based quantum computation[18]. Our work shows that it is feasible to shrink quantum optical experiments to the nanoscale and offers a promising route towards subwavelength quantum optical networks.

In general, a 50/50 beamsplitter transforms two input modes (a_1 and a_2) into two output modes (b_1 and b_2) in such a way that each input is divided equally between the two outputs; that is, a single particle in either input has a 50% chance of ending up in mode b_1 and a 50% chance of ending up in mode b_2. When simultaneously providing a single particle in both input modes, in principle each particle travels independently and four outcomes are possible with equal probability. However, in quantum mechanics these options have to be added coherently, and the rather unexpected result is that for indistinguishable bosons[19] a two-particle interference effect gives only two possible outcomes: either both particles end up in mode b_1 or both in b_2, an effect known as Hong–Ou–Mandel (HOM) interference. Note that, in contrast to classical interference, the intensity, or average number of particles, in either output is not affected and it is just the correlation statistics that change. In terms of quantum operators, the beamsplitter can be described by the transformations $\hat{a}_1 \rightarrow \sqrt{T}\hat{b}_1 + i\sqrt{R}\hat{b}_2$ and $\hat{a}_2 \rightarrow i\sqrt{R}\hat{b}_1 + \sqrt{T}\hat{b}_2$, where R and T denote the reflection and transmission coefficients, and the factor i corresponds to a $\pi/2$ phase shift. Creating a particle simultaneously in modes a_1 and a_2 results in output state $2i\sqrt{RT}(|2\rangle_{b1}|0\rangle_{b2} - |0\rangle_{b1}|2\rangle_{b2}) + (T-R)|1\rangle_{b1}|1\rangle_{b2}$, from which it follows that for an ideal 50/50 beamsplitter the $|1\rangle_{b1}|1\rangle_{b2}$ coincidence term disappears. Although a plasmonic beamsplitter is not lossless, it has been shown theoretically that the interference visibility should remain $2RT/(R^2+T^2)$ as long as the proper beamsplitter phase relations are maintained[20].

The conventional approach for an optical quantum interference measurement is depicted in Fig. 1a. Photons from a photon-pair source are collected in optical fibres and, following a fibre beamsplitter, detected by fibre-coupled silicon avalanche photodiodes (APDs). Alternatively, the photons can be interfered on a bulk dielectric beamsplitter and detected using free-space detectors[17]. In both cases, the complete system is macroscopically large. Dielectric-based integrated optics approaches have managed to shrink such experiments considerably[21,22], but are always limited by diffraction and are still large compared with current electronic components. Plasmonics uniquely offers a larger degree of confinement and therefore allows the creation of structures smaller than the diffraction limit. Our quantum interference scheme in Fig. 1b scales down the whole experiment (except for the source) by several orders of magnitude. In contrast to previous studies[23,24], our beamsplitters are based on directional couplers using the strongly confined waveguide plasmon modes to reach subwavelength length scales.

We used nanofabrication techniques to make our plasmonic beamsplitters and integrated on-chip detectors[16]. This approach is flexible and allows the design of plasmonic networks with parameters obtained from numerical simulations (Supplementary Section SE). A scanning electron microscopy (SEM) image of a typical device is shown in Fig. 2a, together with a zoom-in of the waveguide-coupling region and the detector area. The superconducting single-photon detectors (SSPDs) consist of a meandering line (100 nm width) of a thin (~5 nm) superconducting material (niobium nitride). These devices are operated at 4 K, well below

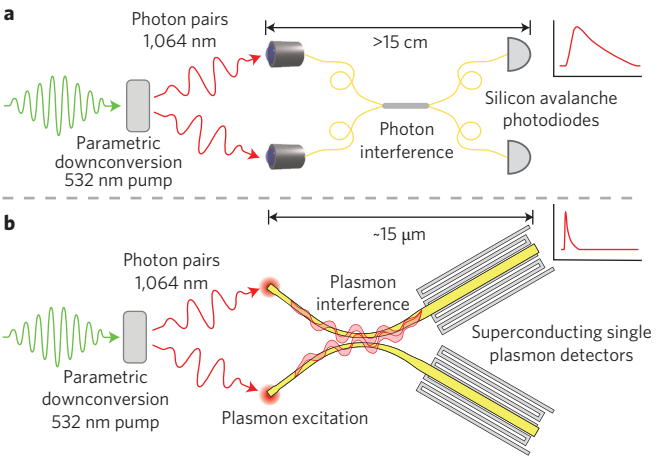

Figure 1 | HOM interference. a, Conventional two-photon quantum interference. Pairs of photons are created in a parametric downconversion process and collected in two optical fibres. Quantum interference takes place in a fibre-based beamsplitter. Photons are measured using silicon APDs. **b**, On-chip plasmon interference. Photon pairs are generated as in **a**, but the interference and detection part of the set-up is several orders of magnitude smaller. A plasmonic directional coupler functions as beamsplitter. SSPDs are integrated to perform near-field detection. The dead time and jitter of SSPDs is much smaller than that of conventional APDs, as indicated schematically by the output signals shown in the insets.

Kavli Institute of Nanoscience, Delft University of Technology, PO Box 5046, 2600 GA Delft, The Netherlands. *e-mail: reinier@heeres.eu

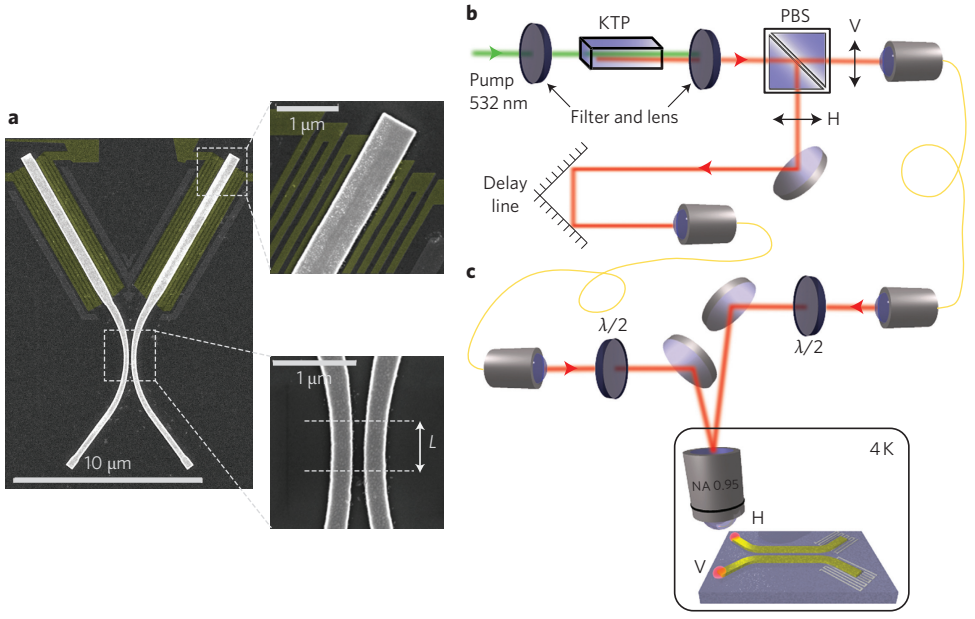

Figure 2 | Plasmon interference device and experimental set-up. a, SEM image of a gold plasmonic directional coupler device. Integrated SSPDs (coloured yellow) are located ~20 nm below the output waveguides. Top-right: zoom-in of the plasmon detection region. The width and spacing of the superconducting meander are both 100 nm and the thickness is ~5 nm. The 150-nm-thick gold waveguide is 600 nm wide and aligned for optimal absorption of the plasmonic mode in the SSPD (Supplementary Fig. S11). Bottom-right: zoom-in of the coupling region, with a waveguide width of 250 nm and gap between waveguides of 100 nm. The cross-coupling ratio can be controlled by varying the interaction length *L*. **b**, Photon-pair source based on degenerate type-II collinear spontaneous parametric downconversion. An ~400 mW pump laser (532 nm) is focused to a ~70-μm-diameter spot in a 2-cm-long potassium titanyl phosphate (KTP) crystal producing photon pairs. The polarizing beamsplitter (PBS) separates the H- and V-polarized photons from a pair to be collected in different optical fibres. A motorized delay line in one of the arms allows the time delay between the two photons to be controlled with ~16 fs resolution. **c**, Experimental set-up. Two beams from optical fibres are focused to separate spots (spot size diameter, ~1 μm) on the sample by a microscope objective. Their polarization can be rotated using half-wave plates to optimize plasmon excitation (Supplementary Fig. S2). Objective and sample are at 4 K in a dipstick filled with helium exchange gas and with a window for free-space optical access.

the critical temperature of ~12 K, by supplying a bias current close to the critical current (~22 μA). After absorption of a single photon, the detector switches locally to the normal, resistive state[15]. The current is shunted to an amplifier and a voltage pulse can be measured. These detectors are easy to operate, sensitive over a broad wavelength range (ultraviolet–near-infrared) and have a very small timing jitter (down to ~50 ps) and dead time (~2 ns).

Optical measurements were performed using the set-up shown in Fig. 2c. We first characterized the plasmon beamsplitter by focusing a laser ($\lambda = 1{,}064$ nm) to a small spot (~1 μm) and raster-scanning this across the device while recording the number of detection events in both detectors simultaneously (Fig. 3a). Plasmon excitation is polarization-sensitive and most efficient with polarization parallel to the waveguide (Supplementary Fig. S2). For the scan we used a linearly polarized beam that couples to both inputs equally. The resulting photoresponse maps in Fig. 3b,c have two very pronounced features. First, the detectors click when directly illuminated due to photon absorption, resulting in the left detector appearing in Fig. 3b and the right detector in Fig. 3c. Second, the two spots in the lower parts of Fig. 3b,c indicate that, when illuminating those positions, both detectors give detection events at an almost equal rate. This signal is caused by coupling into propagating plasmon modes at the end of a single input waveguide. The plasmons are transmitted to both output waveguides approximately equally and then detected by the SSPDs in the near-field. From these measurements we can conclude that the coupling ratio is 0.5 (Supplementary Section SB2).

To create pairs of indistinguishable plasmons we built a bright photon pair source based on a collinear type-II phase-matched degenerate spontaneous parametric downconversion[25] process, as depicted in Fig. 2b. The photon pairs ($\lambda = 1{,}064$ nm, Supplementary Fig. S1) are separated at a polarizing beamsplitter and, after a motorized delay line in one of the arms, a single spatial mode is collected in single-mode fibres. We first characterized the indistinguishability of the produced photon pairs in a HOM experiment using a fibre beamsplitter by performing a time-resolved correlation measurement. The recorded counts versus time t correspond to events where detector 1 clicks, followed by a click from detector 2 at a time t later. For time delays $dt > 3$ ps between the photons, the peak above the uncorrelated background in Fig. 4a around $t = 0$ shows that the counts come from a correlated source; that is, there is an enhanced probability of simultaneous photon detection by the two detectors because our source emits photon pairs. When overlapping the photons in time at the fibre beamsplitter by precisely adjusting the time delay dt, the correlation peak disappears. In this case the photons bunch; that is, they interfere and travel to the same detector, such that there are no correlated clicks between the detectors. In Fig. 4b we plot the integrated area under the curves in Fig. 4a, resulting in the characteristic HOM dip. From the width and depth of the HOM dip we obtain a coherence time $\tau_c = (2.51 \pm 0.03)$ ps and an interference visibility $V = 0.92 \pm 0.01$, limited by non-perfect polarization and spectral overlap.

Next, the H- and V-polarized photons from the photon-pair source are individually coupled to the low-temperature set-up where they are focused to small separate spots (spot size, ~1 μm). After precisely aligning one spot at the left input waveguide and the other at the right waveguide (separation, ~6 μm) and setting the half-wave plates for optimal plasmon excitation, the count rates of the SSPDs are ~45 kHz. The time-resolved correlation data in Fig. 4c now show a much narrower and more pronounced

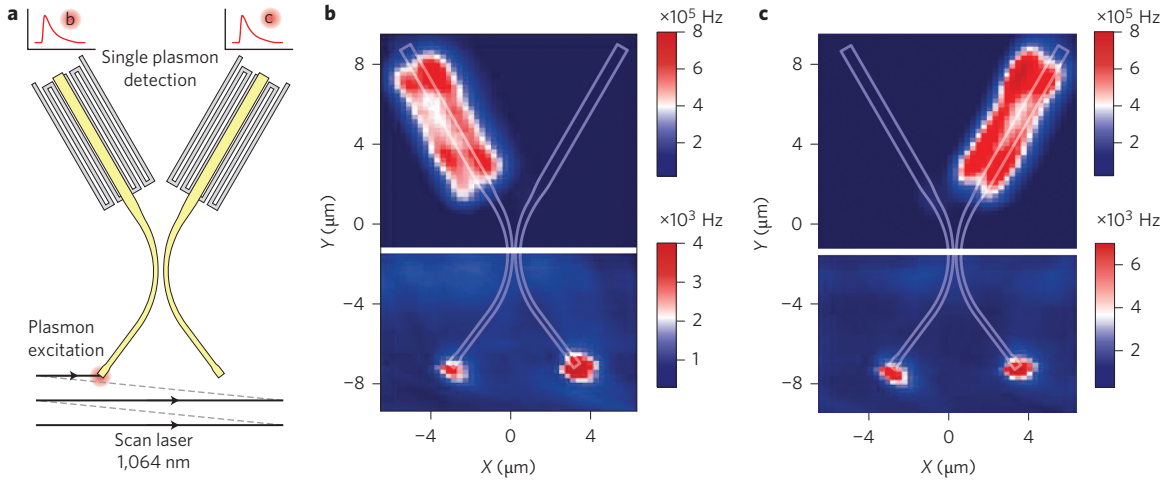

Figure 3 | Photoresponse maps of a plasmonic beamsplitter. a, Measurement procedure: a focused laser beam is raster-scanned across the device. At each location we wait for 0.2 s and count the number of clicks in both the left and right detector. **b**,**c**, Photoresponse maps of a 50/50 plasmonic directional coupler with two SSPDs (device as in Fig. 2a, but with 150 nm gap and $L = 0$). The colour at each pixel represents the number of clicks obtained in the left (**b**) or right (**c**) detector when the laser excitation is at the location of that pixel. The top left of **b** and top right of **c** show that each of the detectors individually clicks very often when directly illuminated, that is, when absorbing photons. The two spots at the bottom of **b** and **c** correspond to plasmons being excited at the ends of the waveguides and reaching both detectors with almost equal intensity, implying a 50/50 coupling strength. Note that different colour scales are used in the upper and lower parts of **b** and **c** because plasmon excitation yields fewer counts due to the limited photon–plasmon coupling efficiency and propagation losses in the waveguide. The laser is linearly polarized and set to excite plasmons with equal intensity at both inputs (approximately vertical with respect to this image). The structure design is superimposed as a guide to the eye.

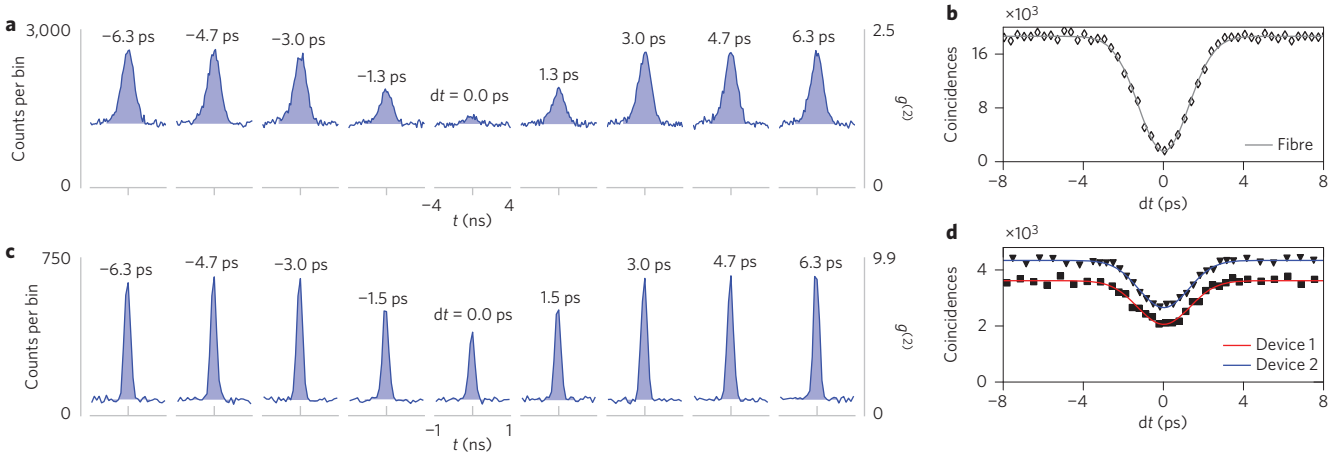

Figure 4 | Quantum interference measurements. a, Time-resolved correlation measurements to characterize the photon-pair source using the scheme in Fig. 1a (fibre beamsplitter-based). The *x*-axis spans the range from −4 to 4 ns, much larger than the interphoton delay *dt* (indicated for each curve). For an interphoton delay of >3 ps, the central peak around $t = 0$, well above the uncorrelated flat background, corresponds to a second-order correlation function $g^{(2)}(0) > 1$ due to the correlated source. The peak width is limited by a jitter of ~600 ps in the APDs. Quantum interference causes these correlations to disappear almost completely when the photons overlap in time. Integration time per curve is 8 s. **b**, HOM interference dip of the photon pair source. The coincidences on the vertical axis are equal to the integrated number of counts at particular delay times *dt* between the two photons from a single pair (that is, shaded areas in **a**). The full-width at half-maximum of the Gaussian fit to the HOM dip gives a coherence time $\tau_c = (2.51 \pm 0.03)$ ps and visibility $V = 0.92 \pm 0.01$. **c**, Time-resolved correlation measurements of plasmon interference using the scheme in Fig. 1b. The *x*-axis now only spans from −1 to 1 ns because the SSPDs have significantly improved timing resolution (jitter, ~120 ps). This results in a lower background and a correspondingly larger $g^{(2)}(0)$. (The time resolution is still larger than the indicated interplasmon delay.) Integration time of 15 min per curve. **d**, HOM interference dip showing quantum interference of surface plasmons in two devices (as shown in Fig. 2a) with a 50/50 directional coupling strength (gap 150 nm, $L = 0$). Coherence time $\tau_c = (2.60 \pm 0.11)$ ps and visibility $V = 0.43 \pm 0.02$ for device 1 (integration time 30 min per point, pairs of traces from **c** combined); $\tau_c = (2.49 \pm 0.08)$ ps and $V = 0.39 \pm 0.01$ for device 2 (integration time 20 min per point). Compared to the photon-pair source properties in **b**, the measured coherence time is identical but the visibility is reduced.

peak above the flat background, again because the detection events come from a correlated source. The improved signal-to-noise ratio is due to the increased time resolution of the SSPDs, which effectively reduces the background signal intensity. We now adjust the time delay between the two plasmons, and again see a decrease in correlated events. The integrated data in Fig. 4d shows the plasmonic HOM dip measured on two different devices, with $\tau_c = (2.60 \pm 0.11)$ ps and $V = 0.43 \pm 0.02$ for device 1 and $\tau_c = (2.49 \pm 0.08)$ ps and

$V = 0.39 \pm 0.01$ for device 2. The interference visibility is reduced by a factor of about 2 in both measured devices. This reduction is due to the simultaneous excitation of long-range surface plasmon modes[26], which are not strongly confined and do not have cut-off. From a polarization-dependent plasmon excitation measurement (Supplementary Fig. S2) we estimate the long-range surface plasmon mode population to be 0.19, which directly translates into a reduced quantum interference visibility $V = 0.49$. Calculations show that imperfect mode overlap in the beamsplitter reduces this value further by 8% (Supplementary Section SE3), bringing the expected value to 0.45, very close to the measured visibilities. However, it is important to observe that the width of the dip is identical to the coherence time of the photon-pair source, implying that the temporal properties of the wave packet are not affected by propagation in the plasmonic mode.

The plasmonic directional couplers we designed in this experiment are significantly smaller than previously realized structures[21–23] and allow further development of subwavelength integrated optical networks with built-in light sources and detectors. This platform provides opportunities to efficiently extract and manipulate photons from single-photon emitters on-chip, without ever converting to a free-space photon. Most importantly, the observation of two-plasmon quantum interference proves that plasmon indistinguishability is maintained and therefore opens the way to implement quantum optical elements at the length scale of typical electronic components.

Methods

Simulations and device design. We performed numerical simulations using an optical mode solver[27]. Mode-dispersion calculations for a single 150-nm-thick waveguide (Supplementary Fig. S5) show that, below a width of ~500 nm, this structure has a single strongly confined mode and two weakly confined long-range modes. We chose a 300-nm-wide, 150-nm-thick waveguide as the basic element of our plasmonic circuit (for mode profile see Supplementary Fig. S6).

In directional couplers, the interaction of the evanescent fields of two nearby waveguides causes their eigenmodes to hybridize into symmetric ($|S\rangle$, Supplementary Fig. S7) and antisymmetric ($|AS\rangle$, Supplementary Fig. S8) combinations called supermodes. Incoming single modes $|L\rangle$ and $|R\rangle$ in the left and right waveguides can be written in the supermode basis: $|L\rangle = 1/\sqrt{2}(|S\rangle + |AS\rangle)$, $|R\rangle = 1/\sqrt{2}(|S\rangle - |AS\rangle)$. Owing to the effective index difference Δn between modes $|A\rangle$ and $|AS\rangle$, the state after propagating over a length Δx is given by $|\psi\rangle = |S\rangle + e^{i2\pi\Delta n\Delta x/\lambda}|AS\rangle$, where λ is the free-space wavelength. When separating this state into modes $|L\rangle$ and $|R\rangle$, the output power oscillates sinusoidally between the left and right waveguide as a function of Δx (measurements in Supplementary Fig. S3). In the case of plasmonic structures, losses give an overall damping factor (for calculations see Supplementary Fig. S10). Based on a trade-off between losses and Δn we selected 250-nm-wide waveguides with a 100 nm spacing to show directional coupler behaviour. The device for the interference measurements had a gap of 150 nm and interaction length $L = 0$ (see Fig. 2a) to operate in the first 50/50 point.

Detection efficiency. The pair production rate of the downconversion source was estimated to be 288 MHz with a fibre collection efficiency of ~35%, based on the measured single and pair rates[28] using silicon APDs with a detection efficiency of ~1.5% at 1,064 nm. Taking into account the transmittance of the objective of ~55% at this wavelength, the overall efficiency of exciting and detecting a plasmon was $\sim 8 \times 10^{-4}$. From simulations and rough calculations we estimate that scattering into the plasmonic mode by focusing a laser at the end of a waveguide has an efficiency of approximately 5–10%.

Received 14 March 2013; accepted 8 July 2013;
published online 11 August 2013

References

1. Barnes, W., Dereux, A. & Ebbesen, T. Surface plasmon subwavelength optics. *Nature* **424,** 824–830 (2003).
2. Schuller, J. *et al.* Plasmonics for extreme light concentration and manipulation. *Nature Mater.* **9,** 193–204 (2010).
3. Chang, D. E., Sørensen, A. S., Hemmer, P. R. & Lukin, M. D. Quantum optics with surface plasmons. *Phys. Rev. Lett.* **97,** 053002 (2006).
4. Oulton, R. *et al.* Plasmon lasers at deep subwavelength scale. *Nature* **461,** 629–632 (2009).
5. Schietinger, S., Barth, M., Aichele, T. & Benson, O. Plasmon-enhanced single photon emission from a nanoassembled metal–diamond hybrid structure at room temperature. *Nano Lett.* **9,** 1694–1698 (2009).
6. Curto, A. G. *et al.* Unidirectional emission of a quantum dot coupled to a nanoantenna. *Science* **329,** 930–933 (2010).
7. Neutens, P., Van Dorpe, P., De Vlaminck, I., Lagae, L. & Borghs, G. Electrical detection of confined gap plasmons in metal–insulator–metal waveguides. *Nature Photon.* **3,** 283–286 (2009).
8. Falk, A. *et al.* Near-field electrical detection of optical plasmons and single-plasmon sources. *Nature Phys.* **5,** 475–479 (2009).
9. Akimov, A. *et al.* Generation of single optical plasmons in metallic nanowires coupled to quantum dots. *Nature* **450,** 402–406 (2007).
10. Kolesov, R. *et al.* Wave particle duality of single surface plasmon polaritons. *Nature Phys.* **5,** 470–474 (2009).
11. Altewischer, E., Van Exter, M. & Woerdman, J. Plasmon-assisted transmission of entangled photons. *Nature* **418,** 304–306 (2002).
12. Fasel, S. *et al.* Energy-time entanglement preservation in plasmon-assisted light transmission. *Phys. Rev. Lett.* **94,** 110501 (2005).
13. Fujii, G. *et al.* Preservation of photon indistinguishability after transmission through surface-plasmon–polariton waveguide. *Opt. Lett.* **37,** 1535–1537 (2012).
14. Chang, D., Sørensen, A., Demler, E. & Lukin, M. A single-photon transistor using nanoscale surface plasmons. *Nature Phys.* **3,** 807–812 (2007).
15. Gol'tsman, G. *et al.* Picosecond superconducting single-photon optical detector. *Appl. Phys. Lett.* **79,** 705 (2001).
16. Heeres, R. W. *et al.* On-chip single plasmon detection. *Nano Lett.* **10,** 661–664 (2010).
17. Hong, C., Ou, Z. & Mandel, L. Measurement of subpicosecond time intervals between two photons by interference. *Phys. Rev. Lett.* **59,** 2044–2046 (1987).
18. Knill, E., Laflamme, R. & Milburn, G. A scheme for efficient quantum computation with linear optics. *Nature* **409,** 46–52 (2001).
19. Loudon, R. Fermion and boson beamsplitter statistics. *Phys. Rev. A* **58,** 4904–4909 (1998).
20. Barnett, S. M., Jeffers, J., Gatti, A. & Loudon, R. Quantum optics of lossy beam splitters. *Phys. Rev. A* **57,** 2134–2145 (1998).
21. Yamada, H., Chu, T., Ishida, S. & Arakawa, Y. Optical directional coupler based on Si-wire waveguides. *IEEE Photon. Technol. Lett.* **17,** 585–587 (2005).
22. Politi, A., Cryan, M. J., Rarity, J. G., Yu, S. & O'Brien, J. L. Silica-on-silicon waveguide quantum circuits. *Science* **320,** 646–649 (2008).
23. Charbonneau, R., Lahoud, N., Mattiussi, G. & Berini, P. Demonstration of integrated optics elements based on long-ranging surface plasmon polaritons. *Opt. Express* **13,** 977–984 (2005).
24. Bozhevolnyi, S., Volkov, V., Devaux, E., Laluet, J. & Ebbesen, T. Channel plasmon subwavelength waveguide components including interferometers and ring resonators, *Nature* **440,** 508–511 (2006).
25. Burnham, D. & Weinberg, D. Observation of simultaneity in parametric production of optical photon pairs. *Phys. Rev. Lett.* **25,** 84–87 (1970).
26. Jung, J., Søndergaard, T. & Bozhevolnyi, S. I. Theoretical analysis of square surface plasmon–polariton waveguides for long-range polarization-independent waveguiding. *Phys. Rev. B* **76,** 035434 (2007).
27. Lusse, P., Stuwe, P., Schule, J. & Unger, H. Analysis of vectorial mode fields in optical waveguides by a new finite difference method. *J. Lightwave Technol.* **12,** 487–494 (1994).
28. Hadfield, R. Single-photon detectors for optical quantum information applications. *Nature Photon.* **3,** 696–705 (2009).

Acknowledgements

The authors thank K. Kuipers and E. Verhagen for discussions, M. Witteveen for help with earlier measurements and R. Zia for discussions and the mode solver code. This work was supported financially by the Netherlands Organisation for Scientific Research (NWO/FOM) and the European Research Council.

Author contributions

R.W.H. designed the experiment, fabricated the samples and performed the measurements and analysis. L.P.K. and V.Z. supervised the project. All authors contributed to the manuscript.

Additional information

Supplementary information is available in the online version of the paper. Reprints and permissions information is available online at www.nature.com/reprints. Correspondence and requests for materials should be addressed to R.W.H.

Competing financial interests

The authors declare no competing financial interests.